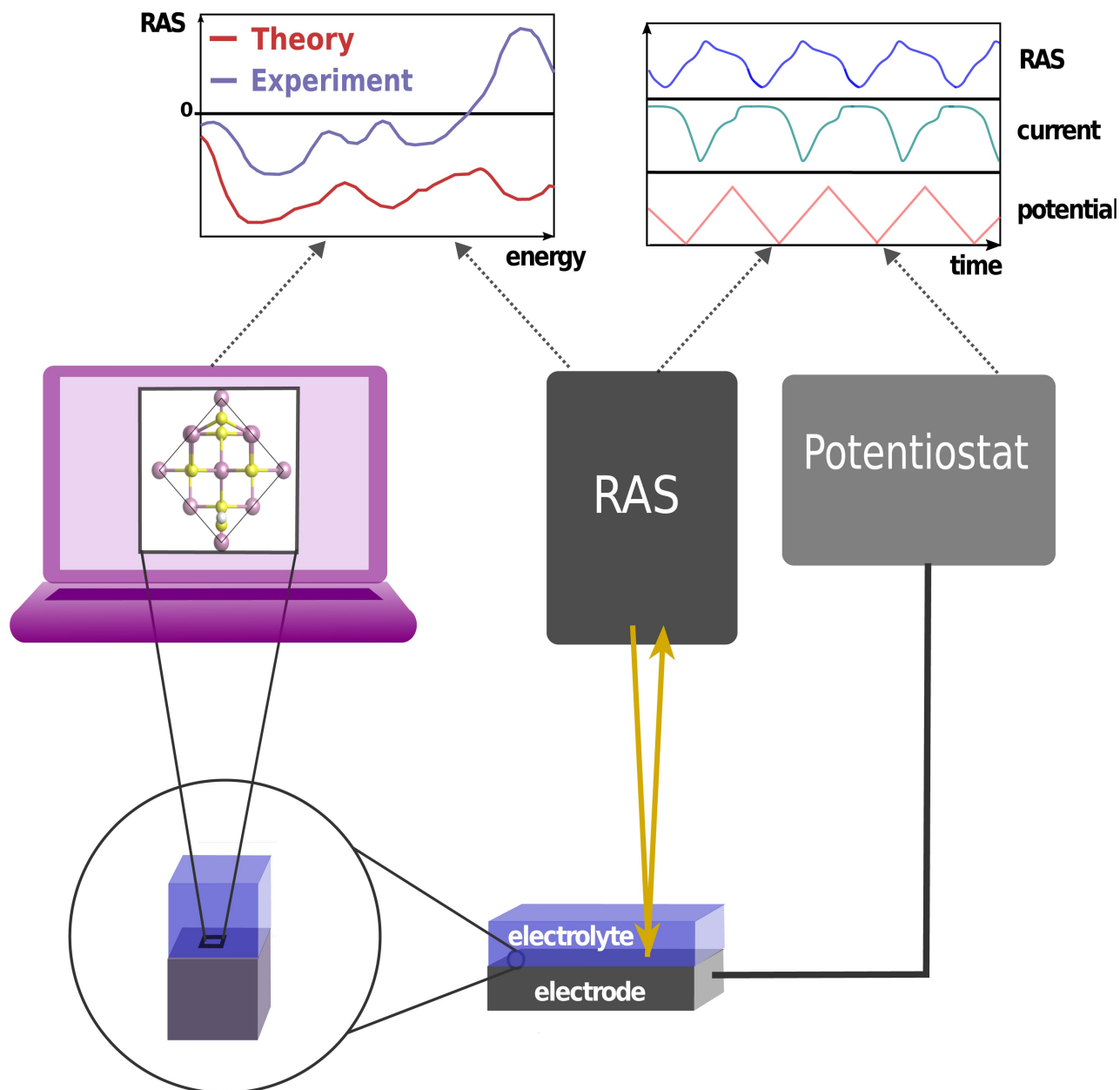


Special
Collection

Experimental and Computational Aspects of Electrochemical Reflection Anisotropy Spectroscopy: A Review

Margot Guidat,^[a, b] Mario Löw,^[b] Moritz Kölbach,^[a] Jongmin Kim,^[a, b] and Matthias M. May*^[a, b]



Electrode/electrolyte interfaces play a crucial role in many electrochemical energy conversion and storage technologies. Hence, a deep understanding of the interfacial structure, energetic alignment and processes is of high relevance and has triggered the development of a number of in situ and operando techniques. One approach for gaining information about the change in surface chemistry and structure on an atomic scale is reflection anisotropy spectroscopy (RAS). This review presents and discusses the continuing effort to develop RAS as an in situ

optical probe for solid-liquid interfaces under applied potentials. Experimental and computational basic principles are presented and key challenges of electrochemical RAS are highlighted. Furthermore, we exemplarily demonstrate the potential of the method for spectroelectrochemistry, focusing on indium phosphide- and gold-aqueous electrolyte interfaces as exemplary case studies, and outline research directions for battery systems.

1. Introduction

Electrochemical energy conversion and storage is expected to play a crucial role in a global sustainable energy system based on renewable energy. Potential applications are for example electrolyzers,^[1] photoelectrochemical (PEC)^[2] as well as photocatalytic water splitting,^[3] batteries^[4], supercapacitors,^[5] and carbon dioxide removal.^[6] At the heart of any of such electrochemical energy conversion and storage systems is the electrode/electrolyte interface. Even though this interface is an essential aspect of improving these devices, the physical and chemical processes occurring at electrochemical interfaces still lack fundamental understanding for most systems.^[7] Changes in the chemistry, morphology and homogeneity of the surface structure of electrodes caused by corrosion, oxidation, and ion ad-/desorption processes can hinder the efficiency and the durability of electrochemical devices.^[8] A microscopic understanding and ultimately controlling and designing the relevant interfaces of (photo)electrodes are hence of particular importance.

Interface and surface phenomena have been widely investigated in ultra-high vacuum (UHV), with techniques such as ex situ X-ray photoelectron spectroscopy (XPS)^[9] and ex situ secondary ion mass spectrometry (SIMS).^[10] However, these methods fail to account for the electrochemical environment and the applied potential at the electrode. An intermediate approach towards a realistic electrochemical environment are emersion-type experiments, where electrodes are exposed to an electrolyte or water film under inert gas conditions, which has to be removed before transfer to an adjacent analysis chamber.^[11] Although recent efforts are focused to further close these gaps by developing techniques such as near-ambient pressure XPS and in situ SIMS,^[12,13] significant challenges remain. Specifically, the short inelastic path of photoelectrons in the electrolyte limits studies to thin film of electrolyte in the case of

ambient pressure XPS, while the utilization of a traditional time-of-flight mass analyzer in SIMS limits the mass resolution.^[14] A deep understanding of the interfacial structure, energetics and processes, however, requires analysis with (close-to) atomic resolution in realistic environments, i.e. with the presence of a thick electrolyte allowing sufficient mass transport for the (photo)currents of a working device.^[15]


The electrochemical double layer (EDL), i.e. the charge distribution at the electrode/electrolyte interface, plays a key role in designing efficient electrodes for electrochemical energy conversion devices. Gaining insight into the EDL requires electrochemical characterization methods with both high time (100 ms or better) and spatial (Å-nm) resolution. The limitation of several techniques with respect to their resolution and the type of information they can provide is described by Esposito et al. in detail.^[8] In short, most experimental methods fall into the two categories of scanning probe measurements (SPM) and pump-probe techniques. The former allow high spatial resolution, but are restricted in temporal resolution. Scanning photocurrent microscopy^[16] and optical spectroscopies (Raman,^[17] Infrared,^[18] UV-visible) are hindered by their optical diffraction resolution ranges and their long acquisition time. The techniques with a higher spatial resolution, i.e. with atomic resolution, are also limited by long acquisition times and by the nature of the interaction, physical by the contact of a tip for atomic force microscopy (AFM)^[19–21] and electrical by the applied voltages for electrochemical scanning tunneling microscopy (ECSTM).^[22] These interactions can alter the surface and hence decrease the reliability of the obtained data. Nevertheless, the time acquisition of scanning probe microscopy techniques can be extended to the millisecond range with video-rate measurements.^[23] Pump-probe techniques consist of ultrafast spectroscopic techniques with a fs-ns time scale for the investigation of electronic processes such as interfacial transfer of charge carriers and lifetimes of electronic and vibrational states.^[24,25] Such techniques show high temporal resolution, but the information is typically non-local.

Another category of techniques that is worth to be mentioned are synchrotron-based X-ray techniques, where the in situ evolution of structural changes of electrodes can be monitored.^[26–28] In addition to be non-destructive, and to have high penetration depth of hard X-rays into liquid electrolytes, surface resonant X-ray diffraction (SRXRD) has the advantage to access the atomic structure of both the electrode and the adsorbate adlayers with a reasonable temporal resolution. Combining these diffraction techniques with additional spec-

[a] M. Guidat, Dr. M. Kölbach, J. Kim, Dr. M. M. May
Institute of Physical and Theoretical Chemistry, Tübingen D-72076,
Germany

[b] M. Guidat, M. Löw, J. Kim, Dr. M. M. May
Universität Ulm, Institute of Theoretical Chemistry, Ulm D-89081, Germany

 An invited contribution to the Electrochemical Nibbles for Computational Chemists Special Collection

 © 2023 The Authors. ChemElectroChem published by Wiley-VCH GmbH. This is an open access article under the terms of the Creative Commons Attribution License, which permits use, distribution and reproduction in any medium, provided the original work is properly cited.

trosopies can give further insight into chemical composition and charge distribution at the electrochemical interface. However, the need to set wavelength and/or polarization state of the X-rays at sufficiently high intensities requires a synchrotron facility. In this review, however, we will focus on lab-based techniques that at least have the potential for a higher sample-throughput and refer the reader to the extensive literature in this field.^[26,27]

In addition to the methods mentioned above, reflection anisotropy spectroscopy (RAS) is a surface-sensitive method that has the potential to help understanding the structure and the fundamental properties of electrochemical interfaces at an atomistic level with an adequate time resolution (down to a few milliseconds).^[29] In short, RAS probes the difference in reflectivity of broad band light at near-normal incidence between two orthogonal directions of a single-crystal surface plane, scaled with the overall reflectivity. An adequate interpretation of experimental RAS data does, however, require both experimental and theoretical considerations to derive a comprehensive understanding of the structure-property relationship of solid-liquid interfaces. To compute the surface optical properties, the surface dielectric function determined from density-functional theory (DFT) is considered.^[30] Some previous studies^[31–33] have already determined the surface optical properties from first principles for the study of surface structure and surface reconstruction in vacuum. In particular, Schmidt et al. have performed many RAS investigations on III–V(100) surfaces in vacuum with quantitative and qualitative analysis.^[34–38] From an electrochemical perspective, however, this approach neglects

effects from the solid surfaces in contact with molecules from a realistic bulk electrolyte.^[39] It is challenging to accurately calculate theoretically derived RAS, since DFT for the underlying ground-state does, in a purely surface-science approach involving vacuum, not necessarily describe the electrode-electrolyte interaction comprehensively. One fundamental challenge consists in including the polarization generated by mobile ions to preserve electric boundary condition from the supercell to the ionic solution.^[40] The main constraints are the simulation of applied electric field and the simulation of realistic electrolyte, limited at best to a mono-layer for large supercells. Model systems with simplified, few-monolayer approximations for electrolytes can, however, be a bridge towards more realistic electrochemical systems.^[39]

In this review, we present and discuss the technique of RAS, with a focus on its development towards an in situ/operando spectroscopy in electrochemical environments. In this regard, the need of method development from an experimental and a computational point of view using well-defined reference systems is highlighted. As case studies, we demonstrate the application of electrochemical RAS for aqueous electrolyte systems with the interfacial structures of indium phosphide and gold in contact with acidic electrolytes. Moreover, we discuss potential applications of RAS to investigate the solid-electrolyte interphase in battery systems.



Margot Guidat is currently a PhD student in physical chemistry at Tübingen University. She received her M.Sc. in chemical engineering from ENSCR at Rennes university in 2020. Her research interests include in situ/operando spectroscopic techniques for elucidating electrochemical processes at solid-liquid interfaces of both solar-water-splitting and aluminum battery systems.



Mario Löw is currently a PhD student at Ulm University. He received his M.Sc. in chemistry from Ulm University in 2021. His research interests include the operando investigation of the interface in rechargeable magnesium batteries.



Jongmin Kim did his PhD studies Humboldt-University of Berlin. He currently holds a postdoctoral position at Tübingen University, where his research focuses on computational investigation of electrochemical interfaces in water-splitting devices as well as further method development within density-functional theory.



Matthias M. May studied physics in Stuttgart, Grenoble, and Berlin, with a focus on condensed matter and computational physics. His PhD studies (2011–2015) at Humboldt-Universität zu Berlin and Helmholtz-Zentrum Berlin targeted III–V semiconductors for solar water splitting. He spent two years as postdoctoral fellow at the Chemistry Department of the University of Cambridge, funded by the German Academy of Sciences Leopoldina. He leads an Emmy-Noether group at the Institute of Physical and Theoretical Chemistry at Tübingen University. His scientific interests lie in the area of photoelectrochemical energy conversion and solid-liquid interfaces.

2. From epitaxial growth to electrochemical interface monitoring

RAS is a linear, differential optic probe that measures the difference in reflectivity of normal incident light between two orthogonal directions of the surface normalized by the overall reflectivity. The definition of the RAS signal is given in equation 1. r_x and r_y are the complex eigenvalues of the Fresnel reflection coefficient tensor along the two axes x and y in the surface plane. In case of an anisotropic surface, r_x and r_y have different values and their difference normalized by the average reflectivity represents the optical anisotropy of the sample.^[41] While both real and imaginary parts are measured, experimental literature typically refers to the real part, a convention that we will also employ for the spectra displayed in the following sections.

$$\text{RAS} = \frac{\Delta r}{r} = 2 \cdot \frac{r_x - r_y}{r_x + r_y} \quad (1)$$

It is noteworthy to mention that one can also probe the anisotropy of the reflectance, i.e. the (real) square of the Fresnel reflection amplitude, $R = |r|^2$. This case is then referred to as reflectance anisotropy spectroscopy, where the relation

$$\text{Re}\left(\frac{\Delta r}{r}\right) \approx \frac{1}{2} \frac{\Delta R}{R} \text{ holds true for } \Delta r \ll r.^{[42,43]}$$

2.1. Experimental realization

The basic working principle of RAS and the configuration used in this study are illustrated in Figure 1. For a more detailed description of the working principle of RAS, we refer the reader to the work of Haberland et al.^[45] When linearly polarized light in the UV-visible range is reflected by an anisotropic crystalline surface, the polarization becomes elliptic and reaches the photoelastic modulator (PEM) of the spectrometer. Due to its birefringent property, the PEM induces a retardation between the two components of the elliptic polarization along the x and y surface crystal direction, resulting in an oscillating signal. After the modulated polarized light has passed through an analyzer, its intensity (I) now depends on the polarization state of the light, the retardation, and the modulation frequency ω of the PEM. This is then detected by a photomultiplier and demodulated by a lock-in amplifier. The intensity, given in equation 2, is thus proportional to the optical ratio shown in the equation 1.^[41]

$$\text{Re}\left(\frac{\Delta r}{r}\right) = \frac{\sqrt{2} I_{2\omega}}{I_0} \quad (2)$$

To allow sufficiently high reflectivity and to limit the complexity of the anisotropic signal, RAS is restricted to single crystals with very low surface roughness (<10 nm). The anisotropy of the signal can arise from both the surface and the bulk of the sample due to the relatively large penetration depth

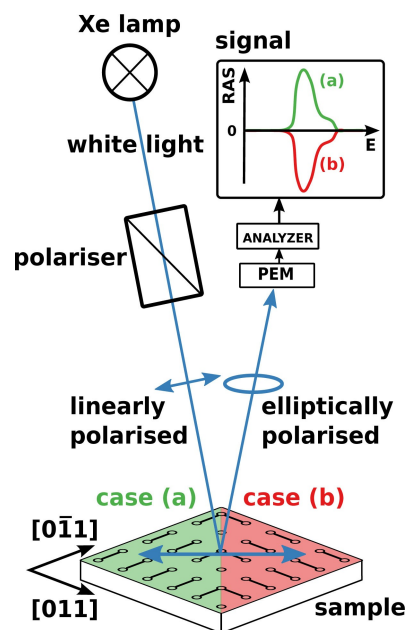


Figure 1. General principle of RAS for the case of a dimerized, cubic (100) surface. The rotation of the dimers by 90° (case a, green vs. case b, red) switches the sign of their contribution to the spectrum. Adapted from Ref. [44] with permission from the ACS. Further re-use subject to permission by ACS.

of light. To get a signal exclusively from the surface, the symmetry of the bulk in the plane of the surface must be isotropic whereas the symmetry of the surface must be anisotropic. Cubic systems with (100) and (111) surfaces orientation have isotropic symmetry and in principle should give a zero RAS signal. However, they can undergo a surface reconstruction. For example, annealing Au(100) allows obtaining a pseudo hexagonal reconstructed Au(100)-(5 × 20) surface which breaks the symmetry between the bulk and the surface and gives a RAS signal exclusively from the surface. For alloys like InP, their surface typically reconstruct in dimer-rich surfaces which present some anisotropy. For cubic systems with (110) surfaces, the RAS signal is more complex because the signal is also arising from the bulk. However, a break in the symmetry between the bulk and the surface gives different contribution to the RAS signal and surface evolution can be monitored. For instance, it is possible to distinguish a (1 × 2) from a (1 × 1) or (1 × 3) reconstruction of Au(110). Yet for example in the case of cubic (100) surfaces, whose bulk is isotropic, it is possible to exclusively get information about the surface.

Several related optical methods currently exist for the study of surface structure and chemistry with a sub-nanometer surface sensitivity. Table 1 shows a summary of the most common of these techniques to distinguish and clarify their differences and similarities with RAS. Surface differential reflectivity (SDR) is very similar, also by name to RAS because the information extracted from both measurements are very similar. However, SDR is applicable for both isotropic and anisotropic surfaces. Since the technique consists of measuring the reflectivity of a sample's surface before and after exposure

Table 1. Main differences between RAS and other related spectroscopic techniques.

Method	RAS	SE ^[a]	SDR ^[b]	ER ^[c]	RAIRS ^[d]
Principle	$2 \cdot \frac{\epsilon_s - \epsilon_b}{\epsilon_s + \epsilon_b}$	$\frac{\epsilon_s}{\epsilon_b}$	$\frac{R_{\text{clean}}(E) - R_{\text{ox}}(E)}{R_{\text{ox}}(E)}$	$a\Delta\epsilon' + b\Delta\epsilon''$	$\int \ln\left(\frac{R_0}{R_{\text{adsorbates}}}\right) d\nu$
Time resolution	few ms	few fs	few ms	few ms	< 1 s
sample type	single-crystal with anisotropic surface	thin film	single-crystal	thin film	single-crystal
typical energy range (eV)	1.5–5	1–6	0.5–5	0.5–5	0.05–0.5
1 or 2 step measurement ?	1 step	1 step	2 steps	2 steps	2 steps

[a] spectroscopic ellipsometry. [b] surface differential reflectivity. [c] electroreflectance. [d] reflection-absorption infrared spectroscopy.

(E) to an external gas (here oxygen as an example in Table 1), the acquisition of one spectrum requires two different experimental conditions. The variation in reflectivity between clean surface and surface after exposure can arise from surface electronic states, electric fields, or optical properties of the growing oxide layer.^[46] Note that although SDR resembles RAS, the type of provided information is different, i.e. SDR allows learning about molecular adsorption, but not about surface ordering and reconstructions.

Spectroscopic ellipsometry (SE) is based on the same principle as RAS. It measures the change of polarization state between the incident and reflected light on a surface. However, while RAS is operating at near-normal incidence, SE is measured at oblique incidence. Therefore, the polarized light is composed of components parallel (rp) and perpendicular (rs) to the plane of incidence. Since the set-up is commonly oriented at 45° from the incidence plane, a signal is emerging from measurements also for isotropic surfaces.^[47,48] This technique is mainly used to determine the dielectric function and the thickness of thin films.^[49]

First introduced by Seraphin,^[50] electroreflectance (ER) is used for the determination of internal parameters of thin-film solar cells such as the internal electric field and the band gaps of the different junctions.^[51] RAS, on the other hand, is a “static” reflection technique which allows accessing the real part of the optical response. While in ER spectroscopy, in addition to the set-up illustrated in Figure 1, an external AC voltage is applied between the backside and the front side of the p-n junction. This applied AC voltage allows accessing both real and imaginary parts of the optical response of the interface, respectively, represented by the real and imaginary part ϵ' and ϵ'' of the dielectric function in Table 1. Thus, the AC voltage “modulates” the reflection, amplifying the response generated by the electric field and suppressing the constant background of reflection.

Finally, reflection-absorption infrared spectroscopy (RAIRS) measures the difference in reflectivity of the surface with ($R_{\text{adsorbates}}$) and without (R_0) adsorbed molecules.^[52,53] Studying adsorbed monolayer and submonolayer on metal surfaces by RAIRS allows accessing information about their molecular structure, their chemical identity and adsorption site.

2.2. Computational aspects

The great challenge for RAS is that, without correlation to other complementary experimental methods, it is not a straightforward quantitative technique. Yet this correlation with other techniques is certainly time-consuming, but sometimes not possible at all. For this reason, complimentary computational efforts are a viable alternative. The following section is not an in-depth picture as can be found in references [41] and [43], but gives a first overview of computational RAS.

Reflection anisotropy is associated with the dielectric response function of a semi-infinite system. According to the three-phase model devised by McIntyre and Aspnes,^[54] the dielectric response function can be described by dielectric functions of bulk and vacuum layers and a surface layer with thickness d .

Equation 1 can be rewritten in the following manner.^[41,43]

$$\frac{\Delta R}{R} = \frac{4\pi d}{\lambda} \text{Im}\left[\frac{\Delta\epsilon_s}{\epsilon_b - 1}\right], \quad (3)$$

where ϵ_s and ϵ_b represent complex dielectric functions ($\epsilon = \epsilon' + i\epsilon''$) of the surface and bulk, respectively, and λ is the wavelength of the light. When the first energy derivative of ϵ_b is employed in this model, it yields to the subsequent equations:

$$\frac{\Delta R}{R} = \frac{4\pi d}{\lambda} [A\Delta\epsilon_s'' - B\Delta\epsilon_s'], \quad (4)$$

where

$$A = \frac{\epsilon_b' - 1}{(1 - \epsilon_b')^2 + (\epsilon_b'')^2}, \quad (5)$$

and

$$B = \frac{\epsilon_b''}{(1 - \epsilon_b')^2 + (\epsilon_b'')^2}. \quad (6)$$

By using the half-slab polarizability α^{hs} , equation 3 transforms into^[55,56]

$$\frac{\Delta R}{R}(\omega) = \frac{4\omega}{c} \operatorname{Im} \left[\frac{4\pi(\alpha_{xx}^{\text{hs}}(\omega) - \alpha_{yy}^{\text{hs}}(\omega))}{\epsilon_b(\omega) - 1} \right]. \quad (7)$$

Likewise, the half-slab polarizability can be applied to equation 4.

For a symmetric slab, α^{hs} can be calculated within the independent-particle random phase approximation (IP-RPA) that neglects the local field effect.^[31]

$$\operatorname{Im} [4\pi \alpha_{xx}^{\text{hs}}(\omega)] = \frac{4\pi^2 e^2}{m^2 \omega^2 A} \sum_{\mathbf{k}} \sum_{v,c} |P_{\mathbf{v}\mathbf{k},\mathbf{c}\mathbf{k}}^x|^2 \times \delta(E_{\mathbf{c}\mathbf{k}} - E_{\mathbf{v}\mathbf{k}} - \hbar\omega). \quad (8)$$

In equation 8, $P_{v,c}$ is the transition matrix element of the momentum operator, and A is the surface area. Calculating this polarizability requires the Kohn-Sham (KS) single-particle eigenvalues and wave-functions. The eigenvalues and wave-functions need to be calculated from DFT or other quantum chemistry methods to be used as an input in the IP-RPA scheme. Unfortunately, this IP-RPA scheme underestimates excitation energies due to the underestimated KS eigenvalues, since the unphysical self-interaction and the derivative discontinuity in the exchange-correlation functional result in an incorrect band gap for semiconductors or insulators. A simple way for correcting this limitation is to consider a scissors shift operator.^[31] This technique is useful for semiconductors or insulators. However, it does not apply to materials where many-body effects are crucial, such as metallic and low-dimensional systems or oxides.

If the slab is nonsymmetric, a real-space cutoff approach to capture the actual surface response is needed. By considering the cutoff θ , modified matrix elements are constructed as follows^[31]

$$\tilde{P}_{\mathbf{v}\mathbf{k},\mathbf{c}\mathbf{k}}^x = -i \int d\mathbf{r} \psi_{\mathbf{v}\mathbf{k}}^*(\mathbf{r}) \theta(z) \frac{\partial}{\partial r_x} \psi_{\mathbf{c}\mathbf{k}}(\mathbf{r}), \quad (9)$$

and the corresponding polarizability becomes

$$\operatorname{Im} [4\pi \alpha_{xx}^{\text{hs}}(\omega)] = \frac{8\pi^2 e^2}{m^2 \omega^2 A} \sum_{\mathbf{k}} \sum_{v,c} [P_{\mathbf{v}\mathbf{k},\mathbf{c}\mathbf{k}}^x]^* \tilde{P}_{\mathbf{v}\mathbf{k},\mathbf{c}\mathbf{k}}^x \times \delta(E_{\mathbf{c}\mathbf{k}} - E_{\mathbf{v}\mathbf{k}} - \hbar\omega). \quad (10)$$

A typical computational workflow to compute equation 7 using equations 9 and 10, which was for instance employed in Refs. [39] and [57], is to start with the structural optimizations of slabs on a DFT level, for instance with the CP2K code,^[58] using the generalized gradient approximation as parameterized by Perdew-Burke-Ernzerhof for the exchange-correlation functional.^[59] The Yambo code^[60,61] readily provides a module for computational RAS in the IP-RPA approach, providing the reflectance, i.e. $\Delta R/R$. Underestimated bandgaps for semiconductors can be corrected by a scissor operator. Using Yambo does, however, require a ground-state calculation in QUANTUM

ESPRESSO^[62] as an intermediate step. For the bulk dielectric function, either experimental or computational input can be employed.

2.3. Application of RAS in surface science

RAS was first developed by Aspnes et al. in the 1980s^[63] to establish an in situ optical probe to achieve a layer-by-layer surface control in III–V semiconductor growth systems as for example molecular beam epitaxy (MBE)^[64] or metal-organic vapor phase epitaxy (MOVPE).^[65] Since then, the technique has been widely used for the study of semiconductor surfaces and interfaces in growth environments. In particular, RAS studies on GaAs have not only demonstrated how the spectroscopy can be used to control epitaxial growth and the preparation of specific surface reconstructions, but also the possibility to investigate layer-by-layer removal of GaAs as a protective cap layer for the preparation of fresh surfaces was shown.^[66–68] More recently, Sombiro et al. have pointed out the utilization of RAS to extract etching rate and etch-depth resolution from the analysis of Fabry-Pérot oscillations generated by reactive ion etching of GaAs/AlGaAs multi-layer structures.^[69] Also dry etching in hydrogen ambient was studied by Brückner et al.,^[70] who report that RAS reveals a layer-by-layer removal from Si(100) single-crystals in H₂ atmosphere at elevated temperatures. This study suggests that RAS is a relevant tool for the development of direct growth processes of III–V/Si solar cells, since well-defined monolayer etching allows single domain preparation. In principle, the fitting methods used to determine growth rate, etching rate, and etch-depth resolution from transients in dry processes can be adapted for transients measured during electrochemical processes.

Investigations on the adsorption of constituents of an electrolyte – typically water – can serve as an intermediate step between UHV and gas-phase studies on the one side and the full electrochemical environment with the solid/liquid phase boundary on the other side.^[44,71–74] The great advantage of such a type of study is that the surface stays in inert gas or vacuum conditions prior to and after water adsorption, which allows to precisely characterize and control the initial surface configuration by standard surface science tools. This can help to understand, for instance, the impact of step edges on the reactivity of a given surface^[74] or derive activation energies.^[71] The downside of such a type of experiment is that the comparability with the realistic electrochemical environment is limited at best. Low-temperature water adsorption from the gas phase^[73] allows to adsorb multi-layer water (ice) on a surface, but reactivity of the interface might be qualitatively different from the ambient temperatures of a typical electrochemical experiment. Adsorption at ambient temperatures, on the other hand, limits the maximum water layer thickness typically to a sub-monolayer.^[44,72] For comprehensive overviews about the application of RAS in a number of fields during the past decades, we refer the reader to the reviews by Weighman et al.^[41] and Supplie et al.^[42] which focus mainly on applications in surface science.

3. Emergence, principles, and application of electrochemical RAS

Implementing (photo)electrochemical surface conditioning for photoelectrodes could enable novel process routes at potentially low costs, but the understanding and control of the related interface (electro)chemistry is so far limited.^[75] Nevertheless, such surface functionalization approaches already demonstrated their use for achieving highest solar-to-hydrogen efficiencies by effective surface protection against corrosion.^[75,76] In this regard, with its straightforward set-up operating at near-normal incidence configuration (Figure 2), RAS represents a

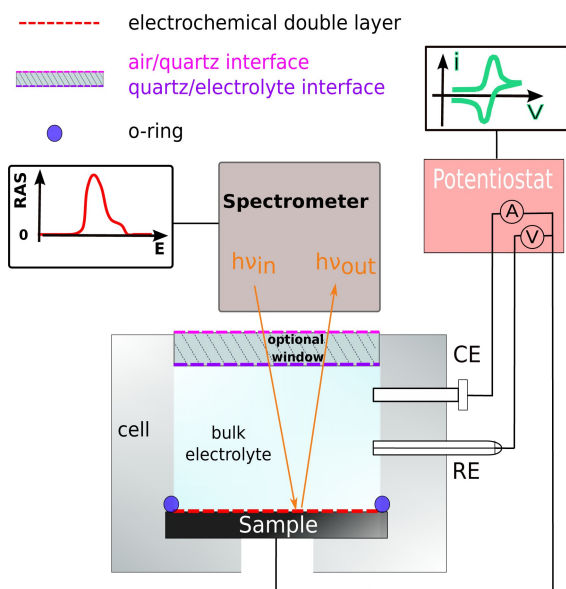


Figure 2. Cross-section of a typical cell setup for electrochemical RAS. CE and RE refer to counter and reference electrode, respectively. Adapted from Ref. [57] with permission from the Royal Society of Chemistry.

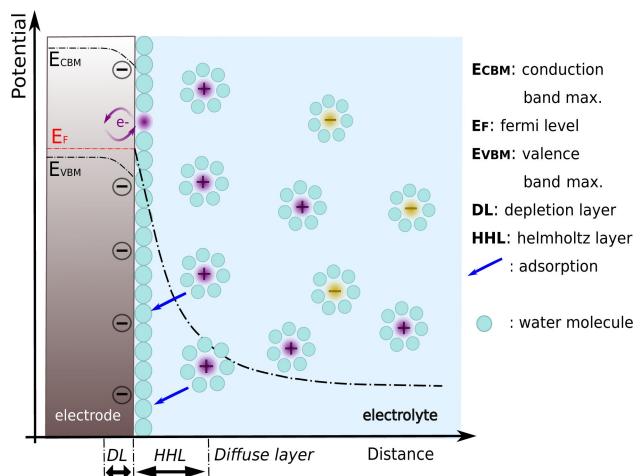


Figure 3. Electrochemical interface of a p-type semiconductor with an electrolyte forming a depletion layer in the dark after equilibrium. The positive and negative charge on the electrolyte side account for solvated ions. Inspired by Gerischer.^[78]

potential tool for the in situ/operando monitoring of (photo)electrochemical surface passivation with a sub-nanometer control of surface modifications.

More generally, RAS can be developed as probe of the electrochemical double layer and can easily be coupled with intrinsically electrochemical characterization methods such as chronoamperometry (CA) or cyclic voltammetry (CV). The correlation between RA spectra and cyclic voltammograms can complement the understanding of electrochemical processes from CV by providing access to charge, potentials, and chemical species with a sub-nanometer spatial resolution in the surface normal. For instance, some surface reconstructions are not distinguishable on the cyclic voltammogram, because they involve non-Faradic processes with very small change in capacitance of the EDL (see Figure 3) and therefore very small charging currents. Thanks to RAS, the different surface reconstructions and surface steps are observable and distinguishable.^[77] In this regard, since the first RAS implementation, there has been a rapid growth of the field and RAS was used on metallic systems in electrochemical environments or molecular films on metals.

3.1. Application of RAS in electrochemistry

Here, we now follow the literature on first “electrochemical RAS” (EC-RAS) applications, i.e. RAS applied in electrochemical environments. First applications of EC-RAS were dedicated to the study of different gold single-crystalline surfaces in aqueous electrolytes. These studies have outlined the relationship between surface charge and reconstruction by measuring RA spectra for interfaces between Au(110) and aqueous electrolytes while potentials were applied to Au(110).^[79,80] Yet, their investigation focused exclusively on experimental EC-RAS and were corroborating previous findings evidenced by STM. Similarly, Sheridan et al. have combined experimental RAS with the modelling of the surface optical response – not full ab initio computational spectroscopy – to investigate the impact of surface phases transition and surface roughening of Au(110) in sulfuric acid under applied voltage on the electronic structure.^[81] Again, to support their findings, the authors refer to results from other studies on the same system, for instance with EC-STM and ex situ low-energy electron diffraction (LEED).^[82,83] This emphasizes that RAS, at least in the initial phase of system exploration, is not a high-throughput technique and that it in principle needs to be supplemented by other surface-sensitive techniques. In such an exploratory phase, it is typically not possible to identify chemical species directly from the spectra. After correlation with complementary experimental techniques or computational spectroscopy, however, an assignment of spectral features to chemical species is often possible.

Mazine et al. combined experimental and computational RAS – the latter for a slab in vacuum – with EC-STM in their study on interfaces of gold with aqueous electrolytes.^[84,85] Correlating STM images and RA spectra show the relationship between surface charge and surface reconstruction and steps, while attempts on including local field effects on theoretical

RAS are made to enlighten the origin of the transitions obtained for the different reconstructions.

In addition to the determination of surface states, surface roughness and surface phase transitions, it is possible to deeply investigate surface transformations, ion adsorption, and solid electrolyte interphase formation processes by evaluating the spectral features during the transition from clean to adsorbate-covered cubic surfaces in both liquid and non-liquid environments. Extensive research on the Cu(110) surface has shown the sensitivity of RAS to molecular adsorbate orientation,^[86,87] and its potential as a surface analytic tool for kinetic studies of molecule adsorption and desorption, as well as their memory effect on the surface.^[88–90] Later on, the study of ad/desorption of molecules in the gas phase on Cu(110) has been extended to electrochemical environments.^[91–93] All studies have mainly investigated chlorine ion adsorption on Cu(110) in hydrochloric acid. Goletti et al. used EC-RAS together with EC-STM and ex situ LEED to identify the two-step process in the anodic and cathodic region of the CV.^[92] They have ruled out the adsorption (desorption) of two different anions and have demonstrated that chlorine anions are involved in one adsorption (desorption) process followed by a surface reconstruction (deconstruction). The latter study on copper has performed EC-RAS on the same system with slightly different potential range and also show together with EC-STM the reversible formation of stripes and channels induced by chlorine ad/desorption.^[93] Very often, specific spectral features of RAS are directly correlated with the surface coverage. By fitting transient measurements with adsorption isotherm models, it is then possible to access some kinetic and thermodynamic quantities.^[74,93] Vazquez-Miranda et al. have particularly demonstrated the extraction of the formation energy of adsorption of chlorine ions and lateral interaction parameter from a transient by fitting it with Frumkin-type isotherms.^[93,94] Furthermore, by correlating the current peaks measured in CV with the derivative of the RAS-transients, they could derive the dependency between applied potential duration and copper/chlorine chemical reactions.

Recently, the use of RAS in combination with AFM and CV has unraveled the mechanism responsible for porphyrin dissolution in acidic media,^[95] a more complex system involving organic molecules. In their approach, several types of porphyrin nanocrystals were vacuum-deposited on graphite substrates and cycled in sulfuric acid. The correlation of RAS with the current density revealed that the single electron transfer involved in the oxidation of porphyrin in a more cationic form is the precursor of its dissolution. The study of porphyrin-liquid interfaces is relevant for energy-storage systems such as post-lithium batteries, where battery based on an alkyne-substituted-porphyrin complex are under development.^[96]

3.2. EC-RAS setup

Figure 2 shows a typical electrochemical RAS setup, where the single-crystal is in contact with the liquid electrolyte. The sample of interest (working electrode) is mounted together with a counter electrode and an optional reference electrode in

a photoelectrochemical cell filled with an electrolyte. Compared to conventional RAS setups, additional potential measurement artefacts in the RA spectrum have to be carefully considered in this configuration, e.g. artefacts from the liquid medium, as the setup now comprises media of at least three different refractive indices, as opposed to two for a vacuum or gas-phase setup. If a quartz window is present in the photoelectrochemical cell, as indicated in Figure 2, it affects the refraction angle of the light at the air-quartz and quartz-electrolyte interfaces due to the different refractive indexes of the media. Hence, the optical path between the spectrometer and the sample has to be carefully adjusted. Furthermore, if non-homogeneous mechanical stress is applied to the window, its dielectric tensor is no longer scalar, leading to a stress-induced contribution of the window to the signal. In principle, the photoelectrochemical cell can also be used without a quartz window. The air-electrolyte interface, however, still changes the refraction angle of the light and hence modifies the light focal point. Also vibration damping might be needed in this case, as vibrations disturb the electrolyte surface and hence the optical path. Baseline effects can be largely compensated by adequate baseline correction using an optically isotropic standard such as an oxidized Si(100) sample, a reference of well-defined anisotropy such as Si(110), or the sum of two spectra where the sample has been rotated by 90° in between.

3.3. Important aspects of the EDL

Literature on electrochemical RAS has so far mainly been limited to metallic systems. This is most likely due to the additional complexity introduced by semiconductor-electrolyte contacts. One factor is almost certainly the reduced structural stability against electrochemical corrosion of most semiconductors when compared to many (noble) metals. Furthermore, the interfacial energetics are altered, as semiconductor-electrolyte interfaces have additional potential drops compared to metal-electrolyte interfaces whose potential drop region is limited (mainly) to the Helmholtz layer (HHL). Figure 3 illustrates a simple case of the electrochemical double layer of solid-liquid interfaces for a semiconductor electrode in the dark. When the semiconductor is in contact with an electrolyte, the charges in the solid need to be redistributed to reach equilibrium due to the Fermi level E_F differences between solution and electrode. The E_F of the semiconductor aligns with the E_F of the red-ox species resulting in a band bending of the conduction and valence band energies (respectively denoted E_{CB} and E_{VB}) forming in this case with a downward band-bending of a p-type semiconductor a depletion layer. Therefore, it is not possible to neglect the tunneling process as for metal electrodes.^[98,99] As sketched in Figure 4, the band bending, which depends on the externally applied voltage/irradiation, the red-ox potential from the electrolyte, and the doping level of the substrate, can shift electronic states of the surface across E_F . Thus, charge transfer between the electrode and the ions adsorbed at the surface can occur via conduction/valence band and via surface states.^[97]

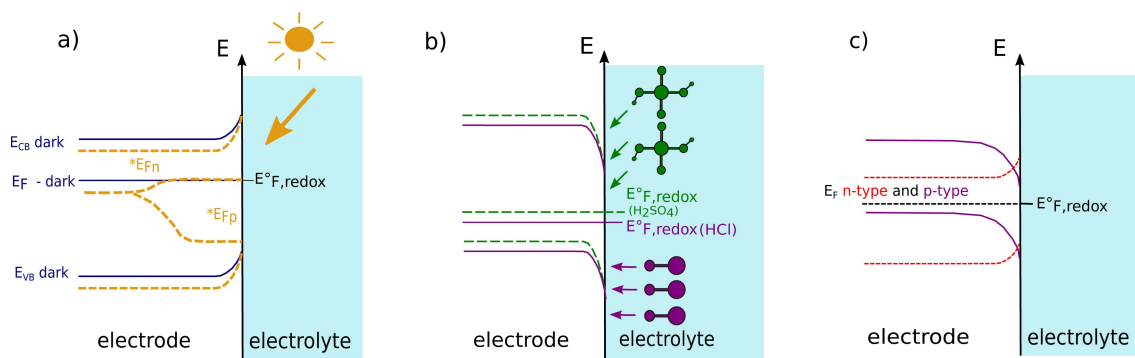


Figure 4. Energetic band diagrams showing the influence of the irradiance, the doping type, and the electrolyte on the EDL and the optical properties of an idealized semiconductor-liquid interface (no surface passivation/corrosion). The electrode is considered as photo-cathode for solar water splitting, and H^+/H_2 is the most active redox couple. Interfacial layers and charge-carrier recombination^[97] are ignored for the sake of simplicity. a) dark and illuminated (dotted line) EDL of n-type semiconductor. b) EDL of p-type semiconductor influenced by the charging effect of H_2SO_4 (dotted lines) and HCl electrolytes (0.01 M). c) EDL for n and p-type semiconductors.

Band bending arises from an electric charge exchange between the bulk and the surface (states) of the semiconductor. The resulting electric field modifies the dielectric function of such a material and therefore contributes to the anisotropy of the associated RA spectrum, making it an indirect probe of interfacial electric fields.^[100] This effect, called the linear electro-optic effect, may have different origins. On the electrode side, the electric field is influenced by the doping level of the substrate, while in the space-charge layer on the electrolyte side, it depends on molecular dipoles and their orientation with respect to the surface, but also on the ion distribution. An electric dipole within an adsorbed molecular film can also affect the integrated electric field. External parameters that impact the electric field are certainly the applied voltage, but also the irradiation of the system. The development of an illumination-induced photovoltage adds another layer of complexity. At a given light intensity, the photovoltage also depends on the charge-carrier recombination, which can, and in most cases will, change upon corrosion or potential-induced restructuring of the interface.^[97] Yet as RAS is an optical technique, a minimum level of illumination by the measurement spot cannot be avoided.

Investigating these different contributions of the electric field by RAS can help elucidate surface reconstructions during molecular chemisorption processes and study preferential adsorption sites from the evidence of adsorbed molecular films.^[101] Taken together, these specifics of the EDL of the semiconductor-electrolyte system show that these interfaces can be more complex than for metals, which also impacts spectroelectrochemistry. Figure 5 compares their different impact on the EDL and on the optical properties of semiconductors. The orange and red spectra, respectively corresponding to n-type with and without additional illumination, are almost identical. It indicates that additional illumination, in the considered situation, has hardly no influence on the optical properties of the interface. In this case, n-type InP is acting as a photo-cathode for the reduction of protons. Hence, as showed on Figure 4 (a), the redox potential aligns with the the quasi-Fermi level of the electrons (${}^{\text{q}}E_{\text{Fn}}$), resulting in a minor increase

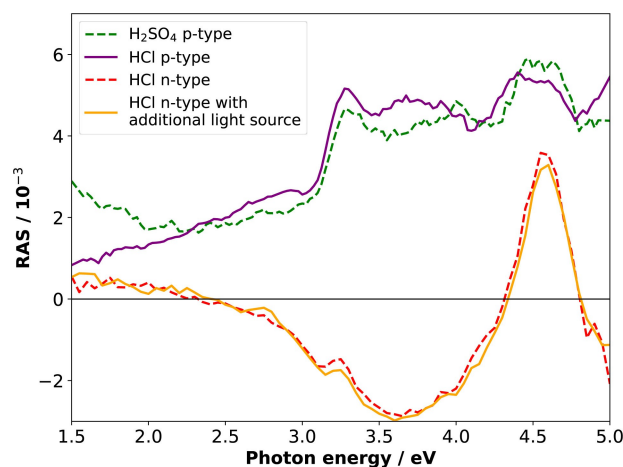


Figure 5. RA spectra of InP(100) for the different conditions a), b) and c) illustrated on Figure 4. Here, the doping shows a major effect, the electrolyte a minor effect, and the bias illumination essentially none.

of the photovoltage. Similarly to the spectra with and without additional illumination, the spectra associated to p-InP-HCl and p-InP- H_2SO_4 interfaces (purple and green spectra, respectively) resemble each other. The electrolytes have the same concentration, but different pH, which influence the redox potential of H^+/H_2 and therefore modify the position of the Fermi level and the band bending (see Figure 4 (b)). For this reason, the type of electrolyte has a minor effect on the related RA spectra. The most noticeable changes between the RA spectra provided by Figure 5 are in fact due to a difference in doping levels. Since E_{CB} , E_{VB} and E_{F} depend on the charge carriers concentrations, the doping level strongly impacts the electronic structure and therefore the optical properties at the interface.

3.4. Aqueous electrolyte systems I: InP(100)

As a first example for the application of electrochemical RAS, we present an investigation of the interfacial structure of InP(100) in contact with 0.01 M hydrochloric acid (HCl). Such

III–V semiconductor/electrolyte interfaces play a crucial role in high-efficiency direct PEC solar water-splitting devices. These systems produce hydrogen via combining water electrolysis and solar energy harvesting in a single process and have been shown to achieve highest solar-to-hydrogen efficiencies.^[75] However, even though significant progress has been made in improving the stability of III–V semiconductors in aqueous electrolytes, corrosion is still preventing practical applications.^[76] Hence, a detailed understanding of the processes at the solid/electrolyte interface is crucial for the realization of a viable solar-water splitting technology based on III–V semiconductors. Therefore, we have chosen InP(100) as a first case study for an electrochemical RAS analysis, as it is available in high single-crystalline quality, but also subject to rapid electrochemical corrosion. A more detailed investigation with experimental details can be found in our recent publication.^[57]

Figure 6 (a) presents a 2D color-coded graphic (colorplot) showing continuously acquired RA spectra in situ under CV conditions. The starting point were samples prepared from *epi-ready* InP(100) wafers, but without pre-treatment of the surface prior to immersion into the electrolyte. The corresponding applied potential as a function of time, and the cyclic voltammogram are shown on the right-hand side of Figure 6

(a) and in Figure 6 (b), respectively. Note that a baseline correction is applied to all the spectra using the signal of an optically isotropic Si(100) crystal in water. Such a continuous type of measurement is helpful for the exploration of a novel system, giving a broad spectral overview at the expense of temporal resolution.

In Figure (b), the cathodic current for the corresponding CV in the voltage range between -0.4 V to -1.3 V can be ascribed to the reduction of InP into phosphine and metallic In. The latter can then further react with HCl to form an InCl interfacial film starting from potentials lower than -0.4 V vs. (Ag/AgCl).^[57] The cathodic current density starting from around -0.4 V and reaching a plateau at -1.3 V is associated with the hydrogen evolution reaction. Here, the current density is limited in rate by the low overall photocurrent from the incident light of the spectrometer, while below -1.7 V, the hydrogen production is no longer photo-current limited.^[57] This highlights again the challenge that for a semiconductor, the optical probe can impact the photoelectrochemical response of the system under investigation.

The formation and disintegration of the InCl film strongly depends on the electrolyte concentration. The literature shows that for high HCl concentration (0.5 M), in the anodic region,

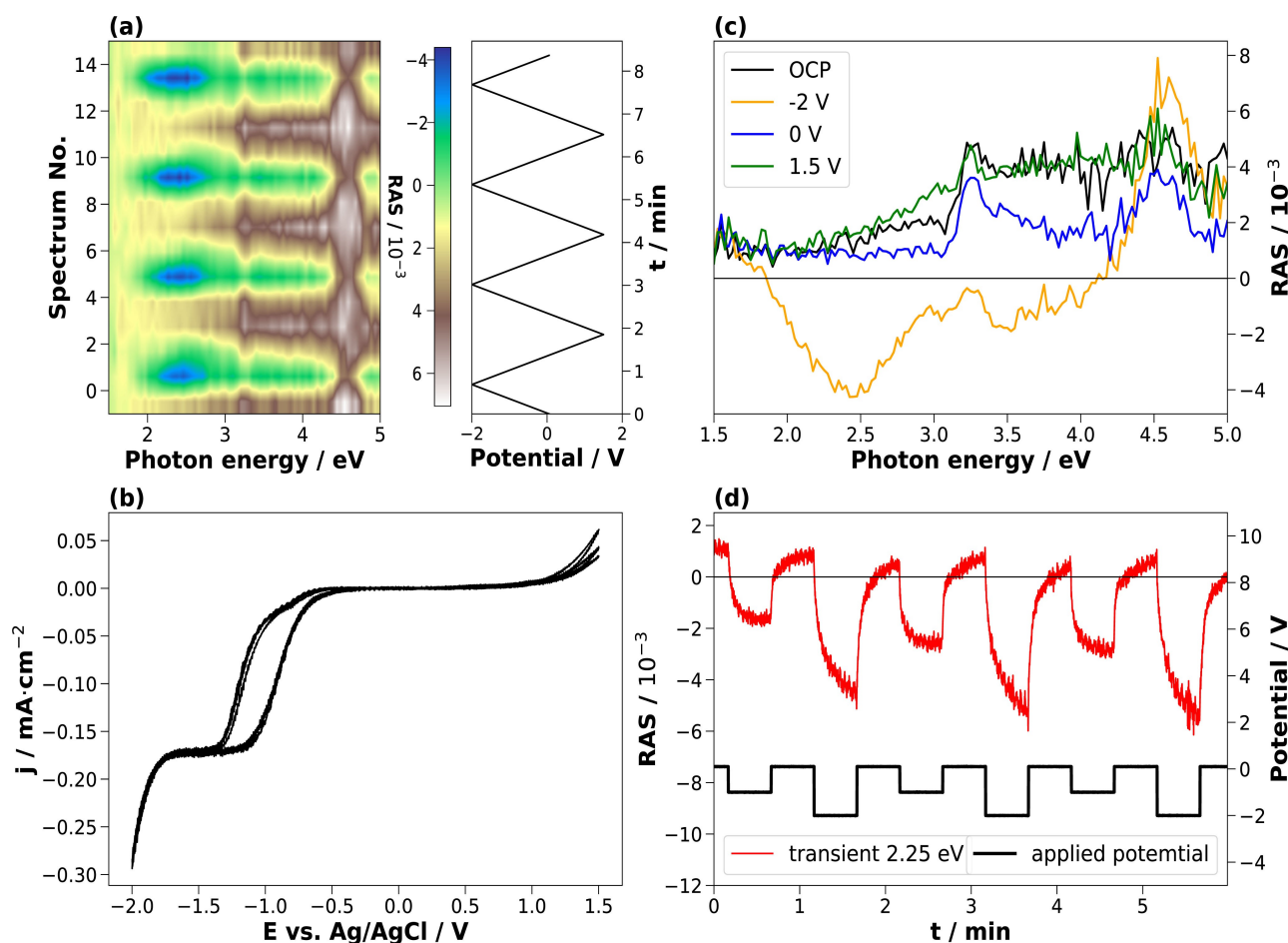


Figure 6. P-type InP(100) in contact with 0.01 M HCl. Left: Colorplot (a) of the InP(100) surface in contact with the electrolyte under cyclic voltammetry conditions (b), scan from open-circuit potential (OCP) towards -2 V and then to 1.5 V for 3 cycles, with a scan rate of 50 mV s⁻¹. Right: RA spectra in the electrolyte (c) at OCP and during chronoamperometry, and transient at 2.25 eV (d) acquired while potential steps are applied.

InCl then only partially dissolves into In^{3+} and Cl^- at -0.3 V vs. (Ag/AgCl). Therefore, the formation of InCl is non-reversible, and a several nm-thick passivation layer builds up over the cycles.^[102–104]

In the case of 0.01 M HCl, however, the CV shows, in terms of the interfacial structure, fully reversible cathodic and anodic processes. The reversibility of the processes is also observed on the colorplot (CP) by a reversible build-up of characteristic anisotropies in the cathodic and anodic potential ranges. The strong anisotropic features shown in Figure 6 (c) indicate well-ordered interfacial structures. A reference spectrum acquired at OCP (around 0.2 V vs. Ag/AgCl) in the electrolyte is plotted together with three spectra measured in 0.01 M HCl at different constant applied potentials. The spectral signature of the reference spectrum exhibits two peaks at around 3.25 and 4.55 eV, respectively, due to surface-modified bulk transitions.^[44] The strong features at about 2.25 and 4.5 eV at -2 V indicate that when scanning to negative potentials, the epi-ready oxide layer present on the epi-ready InP(100) wafer dissolves in the acidic electrolyte, leading to a well-ordered, oxide-free layer. At 0 V and anodic potentials, the spectra are again very similar to the one at OCP, suggesting the re-formation of an oxide layer very similar to the initial epi-ready oxide, accompanied by chlorine-InP interactions.^[103,104] To better understand the involved interfacial structure and chemistry, computational RAS is performed.

Computational RA spectroscopy first requires setting up an adequate selection of structural models for the system under investigation. In this case, the ingredients In, P, O, Cl, and H span a large parameter space of potential structures. Our starting point here was guided by the findings discussed above. For a comparison of computed RA spectra with the experimental spectrum of InP(100) in 0.01 M HCl under the applied potential of -2 V, we consider three structures: the fully Cl^- covered InP(100) surface in which an InCl layer is formed (2Cl), and one and three hydrogen atoms adsorbed on the InP(100) surface (2P-1H and 2P-3H, respectively). Furthermore, we investigate how sensitive the calculated spectrum is to the

adsorption of one and two water molecules on the 2Cl and 2P-1H surfaces. Figure 7 displays the computed spectra of all investigated systems as well as the experimental spectrum. Our calculations reveal that the theoretically derived RA spectra of the 2Cl, 2P-1H, and 2P-3H surfaces are similar to the experimental spectrum. In the 2Cl case, two main negative peaks around 2.2 and 3.8 eV are revealed. The positions of these peaks are slightly changed when the additional one water molecule is adsorbed. The spectral shape, however, remains conserved. The spectrum for two water adsorbed 2Cl surface is considerably up-shifted compared to that of one water adsorbed surface. Interestingly, a positive anisotropy at 4.5 eV, which is observed in the experiment, is not shown. This suggests that the real interface is more complex than a simplified model with a highly ordered supercell and in the absence of oxygen molecules. Similar to the 2Cl structure, we can find the two notable negative anisotropies around 2.5 eV and 3.3 eV in the calculated spectrum of 2P-1H. In contrast to 2Cl, the 2P-1H surface exhibits a strong positive feature at 4.0 eV. This shows a redshift of around 0.55 eV compared to the main positive peak shown in the experiment. The adsorption of water molecules results in a slight blueshift and an increase in the minimum peak. Our calculation of the 2P-3H surface displays a constantly positive feature until 3 eV, a negative anisotropy, and a pronounced positive anisotropy at 3.4 and 4.4 eV, respectively. The corresponding maximum anisotropy in the computed spectrum is similar to that in the experiment. Based on these results, we can anticipate that H-terminated and Cl-terminated surfaces coexist. This hypothesis will have to be tested in future work where applied potentials and more structures are considered.

While the results from computational RAS already help to form a first atomistic picture of the studied electrochemical system, they do not yet show the high degree of quantitative agreement with experiment as often established for many vacuum-based systems. This demonstrates the above-mentioned challenges of the large chemical parameter space resulting in many structures to be considered as well as the

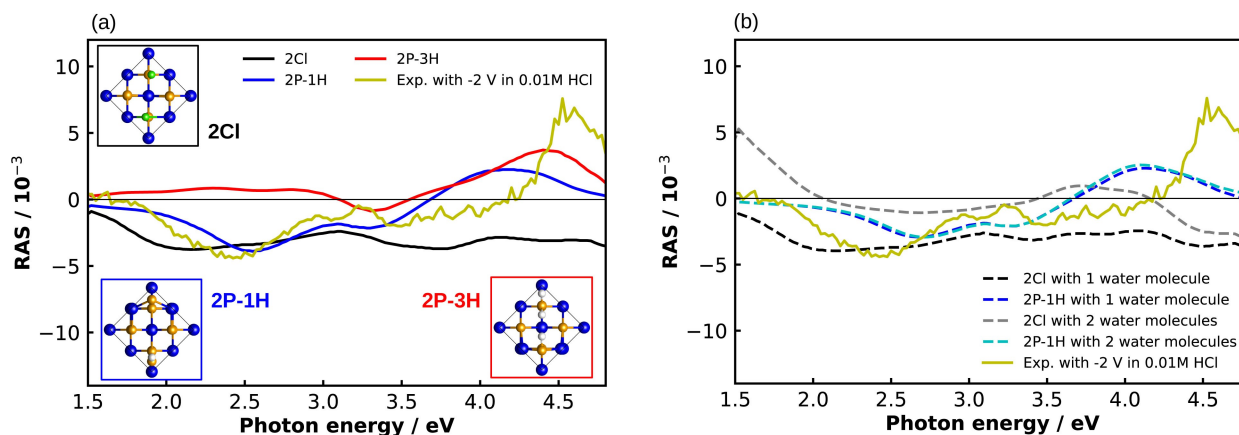


Figure 7. (a) Calculated and experimental (yellow) RA spectra of the InP(100) surface covered with Cl atoms and adsorbed with one and three H atoms. The insets are the top view of corresponding structures. Green-, blue-, orange-, and white-colored balls represent Cl, P, In, and H atoms, respectively. (b) Computed RA spectra of one water molecule adsorbed on 2Cl and 2P-1H.

methodological uncertainty on how to best treat applied potentials in a bulk electrolyte.

Further testing of the validity of the structural model derived from the data above should, in principle, be enabled by complementary XPS, probing the chemical composition of the surface. Yet such an analysis requires the transfer to ultra-high vacuum, where the electrolyte layer has to be removed before the measurement. Yet here, the question arises, if the interfacial layer persists under this change of external conditions. Time-resolved measurements that assess the kinetic stability of a given interface can help to estimate the experimentally available time-window between breaking of the potential control and establishing a dry surface in UHV. Figure 6 (d) shows a transient, where the optical anisotropy is acquired at a fixed photon energy of 2.25 eV, while potential steps at -1 V and -2 V are applied. The fast and reversible change in the anisotropy suggests that if a thin InCl layer builds up in the cathodic region, it immediately dissolves when setting the potential back to OCP. Therefore, at low HCl concentration, the hypothetically formed InCl is unstable and unlikely to be accessible for further analysis by other techniques, where no potential can be applied in an electrolyte, such as XPS in vacuum.

To summarize, in situ electrochemical RAS enabled to identify electrochemical conditions with respect to potentials and electrolyte concentration, under which highly ordered InP-electrolyte interfaces can be prepared. Alas, the observed surface layer generated is not stable when the applied voltage is set back to OCP, which renders complementary analysis for the identification of the exact chemical composition by XPS challenging. The results clearly demonstrate the potential of electrochemical RAS for the monitoring of well-defined (photo)electrochemical etching or layer deposition for III–V semiconductors, especially relevant for solar water splitting applications. In order to computationally identify the real surface structure formed by different potentials, complex surface phase diagram of various surface structures have to be investigated. To do so, molecular dynamics and calculations with applied potentials, followed by excited state calculations can be performed, but the computational effort is significant.

3.5. Aqueous systems II: Au(110)

Understanding electrochemical interfaces implies the ability to distinguish between chemical and physical processes occurring between the electrode surface and the electrolyte. Noble metals such as gold, inert in most acidic and alkaline media, allow focusing on the physical and chemical adsorption of molecules from the electrolyte on the metal surface by preventing or at least – compared to semiconductors – reducing chemical side reactions. Changes in the interaction between the electrolyte's dipoles and electrode surface under applied potentials can also lead to surface structural changes. Insights from these processes on gold can then be ideally transferred to more complex electrochemical systems.

The interfacial structure of gold single-crystals in contact with electrolytes has been experimentally widely investigated by STM, CV, and RAS.^[105,106] Additionally, ex-situ RHEED and LEED have been used in UHV to verify the surface reconstruction after annealing prior to electrochemical cycling.^[107] In particular, Mazine et al. have reported on the reconstruction of Au(110) in sulfuric acid under different applied potentials observed by RAS.^[84] Initially possessing a reconstructed annealed Au(110)(1×2) surface, the crystal adopts an unreconstructed (1×1) surface upon immersion in H₂SO₄. Starting from an Au(110)(1×1) surface in H₂SO₄ at OCP, RAS measurements trace the electrochemically induced surface reconstruction below 0.05 V vs. SCE (0.018 V vs. Ag/AgCl) reference corresponding to a (1×2) missing row. The charge-distribution organization at the electrode surface depends on the applied potential. Hence, tuning the applied potential modifies surface-ion interactions, which play an essential role in the reconstruction/deconstruction.

At room temperature, the unreconstructed Au surface is in a metastable state. Applying a negative electrode potential with respect to the potential of zero charge (pzc) reduces the activation barrier for the reconstruction,^[108] and therefore allows the transition from the (1×1) to the (1×2) surface. When applying potentials above 0.25 V vs. SCE (0.218 V vs. Ag/AgCl), the electrode is charged positively. Adsorption of the anions of the electrolyte (sulfate ions) on the Au surface lifts the reconstruction and the unreconstructed (1×1) surface is restored.

Here, we show typical electrochemical RAS experiments with Au(110) in low concentrations of both sulfuric and hydrochloric acid. Prior to the electrochemical RAS experiment, the crystal is flame-annealed to prepare a reconstructed (1×2) surface.^[79,81,84,108] A baseline correction is applied to all the spectra using the spectrum of Au(110) in the electrolyte at OCP and its inverted spectrum, which was obtained by rotating the sample by 90°. The RA spectra obtained in H₂SO₄ and HCl are presented in Figure 8 (a) and (b), respectively. After annealing, Au(110) RA spectra exhibit a “W”-like shape. Contributions to the complex dielectric function arise both from the bulk and the surface. The slight differences between the spectra are due to different interband transitions from different Fermi level positions.^[80] In general, the results in sulfuric acid (H₂SO₄) agree with those of Mazine et al.^[84] The blue curve was recorded under open-circuit potential and shows a characteristic RA spectrum of well-ordered unreconstructed (1×1) Au(110) in an acidic environment.^[84] The spectra obtained under applied potentials exhibit similar features as the spectrum measured in H₂SO₄. Below OCP, an Au(110) (1×2) reconstruction (-0.15 V, orange spectra) is observed with a pronounced shoulder at about 2 eV. In the range from OCP to 0.6 V, an Au(110) (1×1) unreconstructed (0.3 V, green spectra) surface is existent. This shows that the different surface reconstructions are associated with distinct optical signatures, hence at this stage providing a similar type of information as the diffraction patterns from LEED, which is limited to UHV.

Interestingly, when increasing the potential to values higher than 0.6 V, a positive anisotropic peak develops around 2.3 eV

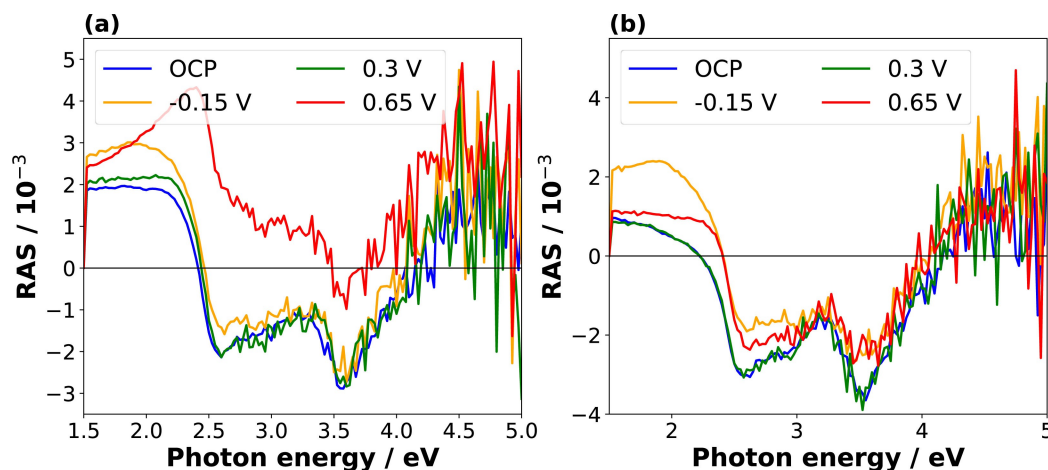


Figure 8. RA spectra of annealed Au(110) in different electrolytes under applied potentials. (a) in 0.1 M HCl and (b) in 0.1 M H₂SO₄ under different applied potentials vs. Ag/AgCl and at OCP. At the beginning of the experiments, the OCP values of Au(110) in 0.1 M HCl in 0.1 M H₂SO₄ were 164 mV and 367 mV, respectively. The orange spectra correspond to the Au(110) (1 × 2) reconstruction while the green spectra correspond to the unreconstructed Au(110) (1 × 1) surface.

in HCl (0.65 V, red spectrum). This peak was not observed in the spectrum measured in H₂SO₄ (see Figure 8 a) and, to the best of our knowledge, has not been reported in the literature. With no computational spectroscopy available at this point, the interpretation of this spectral feature has to rely on literature data. Yet for a metal, this task should be, due to the absence of a photovoltage adding uncertainty to actual potential at the surface as discussed above, a more reliable undertaking.

Some previous studies of gold/acidic electrolyte interfaces have shown that the screening of anions depends on the charge of the surface.^[77,109–111] In particular, Shi et al. have reported that applying a potential above 0.7 V vs. SCE (0.668 V vs. Ag/AgCl) to the Au(111)/HCl interface leads to a change in the polarity of the chemisorption bond between gold and chloride, forming an ordered ($p \times \sqrt{3}$) overlayer of adsorbed chloride.^[111] A polarity drop between Cl⁻ anions and the gold surface could generate a linear electro-optic effect at the Au(110)/HCl interface and could explain the presence of the shoulder on the RA spectrum at 2.3 eV. Furthermore, the formation of an ordered overlayer could explain why the optical anisotropy of the interface is significantly increased. The observed optical anisotropy could therefore be the signature of an ordered Cl⁻ overlayer, formed in the anodic region above 0.7 V vs. SCE (0.668 V vs. Ag/AgCl).

The distinction between anisotropic features responsible for surface reconstructions and electrode/electrolyte electrostatic interactions and the reversibility of these processes can be readily observed in the transient illustrated in Figure 9 (a). The transient corresponds to Au(110) in 0.1 M HCl under CV conditions. Here, the transient was recorded at 2.3 eV because at this energy both features responsible for surface reconstruction/deconstruction and adsorbed anions overlayer are present. The CV, illustrated in Figure 9 (c), was performed between -0.25 V and +0.6 V (vs. Ag/AgCl) with a scan rate of 20 mV/s, starting from -0.25 V for 4 cycles. The current density and the potential from the CV are plotted separately as function of the

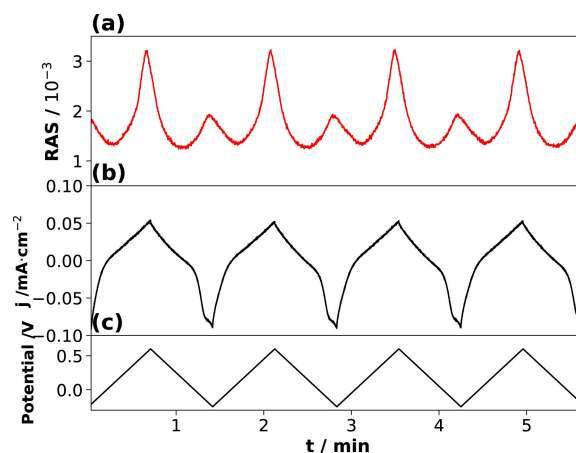


Figure 9. Time-resolved correlation between RAS and CV for Au(110). (a) Transient of Au(110) in 0.1 M HCl at 2.3 eV after annealing, during cycling voltammetry conditions (-0.25 to 0.6 V vs. Ag/AgCl reference electrode for 4 cycles with 20 mV/s scan rate.) (b) and (c) respectively correspond to the current and the voltage as function of the time from the CV.

time on Figure 9 (b) and (c), respectively. Such a plot type allows easier correlation between faradaic processes and changes in optical properties at the interface. The small time shift between the maxima of the current density and the transient is, in this case, an artifact from imperfect temporal alignment of CV and RAS measurements.

Figure 9 (a) shows the first maximum anisotropic peak corresponding to a voltage of 0.6 V and is a signature of the change in chloride adsorption. The second maximum anisotropic peak corresponds to a voltage of -0.25 V and indicates the reconstruction. On the CV, the reconstruction is associated with a progressive decline of the current density from 0.6 to -0.25 V marked by a shoulder at around 0.018 V (vs. Ag/AgCl). Whereas in the same potential range, the anisotropy first decreases until it reaches a minimum at around 0.2 V (beginning of the anion adsorption) and then rises again. The reverse

trend is observed during the deconstruction. Yet, while the transient peaks are almost symmetric around the extrema of the applied potential, the current cycles from the CV show a pronounced asymmetry around the cathodic extremum. After the formation of the reconstruction (below 0.018 V), the slope of the current decrease is reduced towards -0.2 V. This could be attributed either to the onset of a (1×3) surface reconstruction^[112] or a change of the charging current of the EDL. A more detailed analysis of transients during potential steps, also including isotherms^[94] would be needed to clarify this.

In summary, we showed that the well-known, potential-dependent re-ordering of the Au-electrolyte interface is associated with distinct optical anisotropies and can therefore be monitored in a time-resolved manner by electrochemical RAS. This demonstrates how RAS can complement CV, in which the distinction between surface reconstruction and chemical processes is not straightforward. Although electrochemical RAS is more developed for metallic systems than for III–V semiconductors systems – or semiconductors in general – mentioned in the previous section, it still needs significant input to become a well-established method. In this regard, RAS represents an excellent complementary method to scanning tunneling measurements (STM) when investigating single-crystalline metals at different potentials.^[107] It could also be used in the currently field of battery research, especially for metal-anode batteries, as we will briefly discuss in the following.

3.6. Outlook for battery systems

Metal electrodes like magnesium or aluminium are expected to play an essential role in next-generation battery technologies.^[113] Especially for novel material combinations and novel electrolytes, often very little is known about the electrode-electrolyte interface's atomistic structure at operation conditions. Nevertheless, this knowledge is crucial for developing and benchmarking new and sustainable batteries. From this, RAS can potentially be used for battery research on the anode and the cathode, as outlined in the following.

Two aspects are crucial for the investigation of the anode: the solid-electrolyte interphase (SEI) and stripping and plating. For alkali and alkaline earth metals anode batteries, an SEI is formed on the battery's anode in contact with the liquid electrolyte's salts, solvents, additives, or impurities, consisting of different components in either a mosaic, homogeneous or even artificially created form.^[4,114] In addition to the already existing ex situ and in situ/operando techniques for interfaces in batteries,^[115] RAS could be highly beneficial when creating an artificial SEI because it allows controlling the growth process in the same way it monitors the growth process of semiconductors.^[48] The other point worth considering on the anode side is stripping and plating. Here RAS can investigate changes in the surface anisotropy during metal deposition in analogy to epitaxial growth studies in gas-phase ambient.^[48] The technique should also allow the detection of nuclei that lead to dendrite formation. Such investigations are especially

relevant for lithium metal batteries. However, they should also be addressed for multivalent metal batteries (e.g. Al and Mg batteries).^[116]

For the cathode, RAS also promises to benefit battery research: despite a large number of cathode materials for rechargeable magnesium batteries being investigated,^[117] only little is known about the cathode-electrolyte interface (CEI). This is because mostly the intercalation into the cathode is investigated rather than the interphase.^[118] RAS could close the knowledge gap and help develop high-performance batteries by highlighting an often overlooked topic.

However, there are also some challenges when investigating metal electrodes for batteries with RAS, both from an experimental and computational perspective. The first challenge comes with the electrolyte used in batteries, which might be, as in the case of Grignard, optically active.^[119] The consequence is that the probing light is absorbed, which leads to a low signal-to-noise ratio in the RA spectra. Furthermore the surface preparation is quite challenging as alkali and earth-alkaline metals are highly reactive with oxygen and water. Therefore polishing and annealing must be done in a glove box.^[120] This, however, allows for the direct observation of the crystal surface quality without transfer to UHV.

For theoretical investigations, battery electrolytes are also challenging because the number of atoms increases compared to aqueous electrolytes by a factor of ten when using highly advanced electrolytes like $\text{Mg}[\text{B}(\text{hfp})_4]_2$ for magnesium batteries.^[121] Furthermore, for metallic systems, a higher number of k -points are generally demanded to describe partially occupied bands of the systems. These combined effects lead to high computational costs.

As we have outlined, electrochemical RAS for battery applications will be a significant challenge; however, it can open up a new way to investigate the anode and cathode surface operando with a reduced or even without the requirement of correlation with other experimental techniques.

4. Conclusion and Outlook

The present review outlined the potential and current state of RAS as an emerging optical technique for exploring electrochemical interfaces. Probing the polarization state of light reflected at crystalline surfaces, EC-RAS detects changes in the surface structure and surface chemistry of electrochemical systems in situ/operando with a sub-monolayer resolution and on a reasonably fast time scale with standard light sources. The use of more advanced light sources with higher luminosity, hitherto barely explored, could further improve time resolution to the μs range.

Outlining the theory behind computational RAS, we briefly showed that standard DFT on a PBE level together with IP-RPA for the excited states can already provide reasonable, quantitative results for some systems. While in general, the computational method is relatively well-established for semiconductors, it remains challenging for metallic systems, whereas for electrochemical experiments, the study of metals dominates. Further-

more, the exploration of best practices for computational RAS of electrochemical systems has just begun. This explains why most EC-RAS applications on metallic systems in the literature combined their studies with other experimental techniques such as STM, but none used computational RAS.

We presented typical experimental approaches and results for the metallic system Au(110) and the semiconductor InP(100). For the former, RA spectra under applied potentials show that RAS is a powerful tool to visualize changes in surface reconstruction and in ions adsorption at the interface. For the latter, we also show first steps for the interpretation of experimental signatures aided by computational spectra derived from a DFT ground-state structure. This already allowed to determine experimental parameters with respect to applied potential and electrolyte composition, at which ordered surfaces of InP can be stabilized in the electrolyte, providing a starting position for further (photo)electrochemical surface processing. Yet the many constituents of the interface in addition to the requirement to apply an electrode potential in a realistic manner renders the configuration space to be probed by DFT large and the overall computational effort significant.

Time-resolved potential steps measurements allow to quantify the time-window available between breaking of the potential control and complete removal of the electrolyte for transfer to complementary UHV-based analysis. This is highly relevant to assess the transferability decoupled electrochemical experiments followed by surface science analysis in vacuum. Furthermore, fitting time-resolved measurements with adsorption isotherm models gives more quantitative insights into interfacial processes by the determination of kinetic and thermodynamic parameters. Also quantitative measures for the surface quality prior to or during an electrochemical experiment can be derived. When comparing a specific spectrum with a reference spectrum for the same surface, it is possible to quantitatively assess the quality of a given surface, i.e. which fraction of the surface actually shows a given reconstruction. Similarly, the quantity of a specific chemical species or ion on a well-ordered interface can be assessed, as soon as the corresponding spectral signature has been identified from complementary experiments or computational spectroscopy. Finally, RAS also has the potential to make an impact in battery research, giving insides into SEI formation, metal stripping and plating, as well as ion transport processes.

Experimental Section

InP samples were prepared from p-doped InP(100) (Zn-doping of $4 \cdot 10^{18} \text{ cm}^{-3}$), single-crystalline wafers with an offcut of $(0 \pm 0.5)^\circ$ from CrysTec. The wafers with an epi-ready surface were cleaved and used without further pre-treatment. For the RAS measurement, the InP samples were mounted into a photoelectrochemical cell (PECC) from Zahner without an optical window. The back-side of the samples were contacted with a copper wire, fixed with a silver paste (Ferro GmbH), and with Galn eutectic (Sigma Aldrich). Pt and Ag/AgCl electrodes were used as counter and reference electrodes, respectively.

A gold single crystal was purchased from Mateck (purity 99,999%), polished on one side to a roughness below $0.01 \mu\text{m}$ and an orientation accuracy better than 0.1° . Before electrochemical RAS measurements, the crystal was flame-annealed with the following procedure. The crystal was placed on a ceramic plate and flamed annealed with a bunsen burner gun to about 100°C below the melting temperature for about 5 minutes until the edge of the crystal turned red. The crystal was cooled down under Argon flow for about 10 min.^[122] The annealed crystal was then transferred to the PECC equipped with an optical window. Pt and Ag/AgCl electrodes were used as counter and reference electrodes, respectively.

The PECC was filled with the HCl and H_2SO_4 electrolytes (VWR Chemicals, reagent grade). The RA spectra were measured with an RA-Spectrometer (EpiRAS from Laytec) equipped with a Xenon light source. The electrochemical measurements were done with a potentiostat (Versa STAT 3F from AMETEK). Further details of the experimental procedure can be found elsewhere.^[57]

For structural optimizations of slabs of the electronic structure model, DFT calculations were performed using the CP2K code.^[58] The code employs the gaussian and plane waves scheme. The generalized gradient approximation (GGA) as parameterized by Perdew-Burke-Ernzerhof (PBE) for the exchange-correlation functional was used.^[59] A plane-wave cutoff of 800 Ry was set. We adopted Goedecker-Teter-Hutter (GTH) pseudopotentials. Ground-state properties were computed with QUANTUM ESPRESSO.^[62] Here, we employed optimized norm-conserving vanderbilt pseudopotentials.^[123] The sampling of Brillouin zone (BZ) was carried out with a $10 \times 10 \times 1$ k-grid, and an energy cutoff was set to 60 Ry. For computational RAS, we used the IP-RPA approach implemented in Yambo.^[60,61] We applied a scissor operator to correct the underestimated band gap.

Acknowledgements

The following organizations are thanked for financial support: DFG (Deutsche Forschungsgemeinschaft) under Germany's Excellence Strategy – EXC 2154 – Project number 390874152 as well as DFG project number 434023472. Computational resources were provided by the state of Baden-Württemberg, through bwHPC, and DFG through grant no. INST 40/575-1 FUGG (JUSTUS 2 cluster). We thank Krishnaveni Palanisamy for discussions on the experimental approach to anneal the gold crystals.

Conflict of Interest

The authors declare no conflict of interest.

Data Availability Statement

The data used to generate the plots for this review (section 3) are openly available on Zenodo^[124] and the NOMAD Repository.^[125]

Keywords: electrochemistry · interfaces · time-resolved spectroscopy · computational chemistry · surface chemistry

- [1] M. Chatenet, B. G. Pollet, D. R. Dekel, F. Dionigi, J. Deseure, P. Millet, R. D. Braatz, M. Z. Bazant, M. Eikerling, I. Staffell, P. Balcombe, Y. Shao-Horn, H. Schäfer, *Chem. Soc. Rev.* **2022**, *51*, 4583.
- [2] K. Sivula, R. van de Krol, *Nat. Rev. Mater.* **2016**, *1*, 15010.
- [3] Q. Wang, K. Domen, *Chem. Rev.* **2020**, *120*, 919.
- [4] J. Popovic, *Nat. Commun.* **2021**, *12*, 6240.
- [5] J. Sun, B. Luo, H. Li, *Adv. Sustainable Syst.* **2022**, *3*, 2100191.
- [6] M. M. May, K. Rehfeld, *Adv. Energy Mater.* **2022**, *12*, 2103801.
- [7] M. Wang, Z. Feng, *Chem. Commun.* **2021**, *57*, 10453.
- [8] D. V. Esposito, J. B. Baxter, J. John, N. S. Lewis, T. P. Moffat, T. Ogitsu, G. D. O'Neil, T. A. Pham, A. A. Talin, J. M. Velazquez, B. C. Wood, *Energy Environ. Sci.* **2015**, *8*, 2863.
- [9] M. Bozorgchenani, F. Buchner, K. Forster-Tonigold, J. Kim, A. Groß, R. J. Behm, *Langmuir* **2018**, *34*, 8451.
- [10] C. R. Brundle, Ultra-High Vacuum Techniques of Surface Characterization, in *Industrial Applications of Surface Analysis*, volume 199 of ACS Symposium Series, pages 13–32, American Chemical Society **1982**.
- [11] A. Hajduk, M. V. Lebedev, B. Kaiser, W. Jaegermann, *Phys. Chem. Chem. Phys.* **2018**, *20*, 21144.
- [12] D. M. Itkis, J. J. Velasco-Velez, A. Knop-Gericke, A. Vyalikh, M. V. Avdeev, L. V. Yashina, *ChemElectroChem* **2015**, *2*, 1427.
- [13] Z. Wang, Y. Zhang, B. Liu, K. Wu, S. Thevuthasan, D. R. Baer, Z. Zhu, X.-Y. Yu, F. Wang, *Anal. Chem.* **2016**, *89*, 960.
- [14] M. Favaro, B. Jeong, P. N. Ross, J. Yano, Z. Hussain, Z. Liu, E. J. Crumlin, *Nat. Commun.* **2016**, *7*, 12695.
- [15] S. Axnanda, E. J. Crumlin, B. Mao, S. Rani, R. Chang, P. G. Karlsson, M. O. M. Edwards, M. Lundqvist, R. Moberg, P. Ross, Z. Hussain, Z. Liu, *Sci. Rep.* **2015**, *5*, 9788.
- [16] D. V. Lang, C. H. Henry, *Solid-State Electron.* **1978**, *21*, 1519.
- [17] R. Paul, G. Safa, G. Dina, *J. Raman Spectrosc.* **2016**, *6*, 16.
- [18] W. S. Lau, *Infrared Characterization for Microelectronics*, World Scientific **1999**.
- [19] D. Cao, Y. Song, J. Peng, R. Ma, J. Guo, J. Chen, X. Li, Y. Jiang, E. Wang, L. Xu, *Front. Chem.* **2019**, *7*, 626.
- [20] Y. Gan, G. V. Franks, *J. Phys. Chem. B* **2005**, *109*, 12474.
- [21] A. Jarzemski, C. Shaskey, K. Park, *Front. Energy* **2018**, *12*, 43.
- [22] M. Aliofkhaezrai, *Modern Electrochemical Methods in Nano, Surface and Corrosion Science*, IntechOpen, Rijeka **2014**.
- [23] O. M. Magnussen, *Chem. Eur. J.* **2019**, *25*, 12865.
- [24] M. Maiuri, M. Garavelli, G. Cerullo, *J. Am. Chem. Soc.* **2020**, *142*, 3.
- [25] T. Elsaesser, *Chem. Rev.* **2017**, *117*, 10621.
- [26] H. Khan, A. S. Yerramilli, A. D'Oliveira, T. L. Alford, D. C. Boffito, G. S. Patience, *The Canadian Journal of Chemical Engineering* **2020**, *98*, 1255.
- [27] B. F. Baggio, Y. Gründer, *Annual Rev. Anal. Chem.* **2021**, *14*, 87.
- [28] K. A. Stoerzinger, W. T. Hong, E. J. Crumlin, H. Bluhm, Y. Shao-Horn, *Acc. Chem. Res.* **2015**, *48*, 2976.
- [29] R. J. Gale (Editor), *Spectroelectrochemistry*, Springer US **1988**.
- [30] A. Groß, *Theoretical Surface Science*, Springer, Berlin, Heidelberg **2009**.
- [31] C. Hogan, R. Del Sole, G. Onida, *Phys. Rev. B* **2003**, *68*, 035405.
- [32] C. Hogan, E. Ferraro, N. McAlinden, J. F. McGill, *Phys. Rev. Lett.* **2013**, *111*, 087401.
- [33] C. Hogan, R. Magri, R. Del Sole, *Phys. Rev. B* **2011**, *83*, 155421.
- [34] W. G. Schmidt, K. Seino, P. H. Hahn, F. Bechstedt, W. Lu, S. Wang, J. Bernholc, *Thin Solid Films* **2004**, *455–456*, 764.
- [35] W. G. Schmidt, J. L. Fattebert, J. Bernholc, F. Bechstedt, *Surf. Rev. Lett.* **1999**, *06*, 1159.
- [36] W. G. Schmidt, A. Hermann, F. Fuchs, M. Preuss, *Large-Scale Simulations for Understanding Surface Optical Spectra*, Springer-Verlag **2006**.
- [37] W. G. Schmidt, F. Bechstedt, J. Bernholc, *J. Vac. Sci. Technol. B* **2000**, *18*, 2215.
- [38] W. G. Schmidt, N. Esser, A. M. Frisch, P. Vogt, J. Bernholc, F. Bechstedt, M. Zorn, T. Hannappel, S. Visbeck, F. Willig, W. Richter, *Phys. Rev. B* **2000**, *61*, R16335.
- [39] M. M. May, M. Sprik, *New J. Phys.* **2018**, *20*, 033031.
- [40] C. Zhang, T. Sayer, J. Hutter, M. Sprik, *J. Phys. E* **2020**, *2*, 032005.
- [41] P. Weightman, D. S. Martin, R. J. Cole, T. Farrell, *Rep. Prog. Phys.* **2005**, *68*, 1251.
- [42] O. Supplie, M. M. May, S. Brückner, N. Brezhneva, T. Hannappel, E. V. Skorb, *Adv. Mater. Interfaces* **2017**, *4*, 1601118.
- [43] W. G. Schmidt, *Phys. Status Solidi B* **2005**, *242*, 2751.
- [44] M. M. May, H.-J. Lewerenz, T. Hannappel, *J. Phys. Chem. C* **2014**, *118*, 19032.
- [45] K. Haberland, P. Kurpas, M. Pristovsek, J.-T. Zettler, M. Weyers, W. Richter, *Appl. Phys. A* **1999**, *68*, 309.
- [46] A. Cricenti, *J. Phys. Condens. Matter* **2004**, *16*, S4243.
- [47] A. Rothen, *Rev. Sci. Instrum.* **1945**, *16*, 26.
- [48] J.-T. Zettler, *Prog. Cryst. Growth Charact. Mater.* **1997**, *35*, 27.
- [49] S. Richter, O. Herrfurth, S. Espinoza, M. Rebarz, M. Kloz, J. A. Leveille, A. Schleife, S. Zollner, M. Grundmann, J. Andreasson, R. Schmidt-Grund, *New J. Phys.* **2020**, *22*, 083066.
- [50] B. O. Seraphin, *Optical Properties of Solids: Papers from the NATO Advanced Study Institute on Optical Properties of Solids*, Springer US **1969**.
- [51] C. Huber, C. Krämmer, D. Sperber, A. Magin, H. Kalt, M. Hetterich, *Phys. Rev. B* **2015**, *92*, 075201.
- [52] P. Hollins, *Infrared Reflection–Absorption Spectroscopy*, John Wiley & Sons, Ltd, Chichester, UK **2006**.
- [53] K. Mudiyansele, D. J. Stacchiola, *In-situ Infrared Spectroscopy on Model Catalysts*, John Wiley and Sons, Inc. **2013**.
- [54] J. McIntyre, D. Aspnes, *Surf. Sci.* **1971**, *24*, 417.
- [55] R. del Sole, *Solid State Commun.* **1981**, *37*, 537.
- [56] F. Manghi, R. Del Sole, A. Selloni, E. Molinari, *Phys. Rev. B* **1990**, *41*, 9935.
- [57] M. Löw, M. Guidat, J. Kim, M. M. May, *RSC Adv.* **2022**, *12*, 32756.
- [58] T. D. Kühne, M. Iannuzzi, M. D. Ben, V. V. Rybkin, P. Seewald, F. Stein, T. Laino, R. Z. Khaliullin, O. Schütt, F. Schiffrmann, D. Golze, J. Wilhelm, S. Chulkov, M. H. Bani-Hashemian, V. Weber, U. Borštnik, M. Taillefumier, A. S. Jakobovits, A. Lazzaro, H. Pabst, T. Müller, R. Schade, M. Guidon, S. Andermatt, N. Holmberg, G. K. Schenter, A. Hehn, A. Bussy, F. Belleflamme, G. Tabacchi, A. Glöb, M. Lass, I. Bethune, C. J. Mundy, C. Plessl, M. Watkins, J. VandeVondele, M. Krack, J. Hutter, *J. Chem. Phys.* **2020**, *152*, 194103.
- [59] J. P. Perdew, K. Burke, M. Ernzerhof, *Phys. Rev. Lett.* **1996**, *77*, 3865.
- [60] A. Marini, C. Hogan, M. Grüning, D. Varsano, *Comput. Phys. Commun.* **2009**, *180*, 1392.
- [61] D. Sangalli, A. Ferretti, H. Miranda, C. Attaccalite, I. Marri, E. Cannuccia, P. Melo, M. Marsili, F. Paleari, A. Marrazzo, G. Prandini, P. Bonfà, M. O. Atambo, F. Affinito, M. Palumbo, A. Molina-Sánchez, C. Hogan, M. Grüning, D. Varsano, A. Marini, *J. Condens. Matter Phys.* **2019**, *31*, 325902.
- [62] P. Giannozzi, S. Baroni, N. Bonini, M. Calandra, R. Car, C. Cavazzoni, D. Ceresoli, G. L. Chiarotti, M. Cococcioni, I. Dabo, A. D. Corso, S. de Gironcoli, S. Fabris, G. Fratesi, R. Gebauer, U. Gerstmann, C. Gougoussis, A. Kokalj, M. Lazzeri, L. Martin-Samos, N. Marzari, F. Mauri, R. Mazzarello, S. Paolini, A. Pasquarello, L. Paulatto, C. Sbraccia, S. Scandolo, G. Sciauzero, A. P. Seitsonen, A. Smogunov, P. Umari, R. M. Wentzcovitch, *J. Phys. Condens. Matter* **2009**, *21*, 395502.
- [63] D. E. Aspnes, A. A. Studna, *Phys. Rev. Lett.* **1985**, *54*, 4.
- [64] B. A. Joyce, *Rep. Prog. Phys.* **1985**.
- [65] M. Behet, R. Hövel, A. Kohl, A. M. Küsters, B. Opitz, K. Heime, *Microelectronics J* **1996**, *27*, 297.
- [66] Z. Sobiesierski, D. I. Westwood, M. Elliott, *Phys. Rev. B* **1997**, *56*, 15277.
- [67] J. Ortega-Gallegos, L. Guevara-Macías, A. Ariza-Flores, R. Castro-García, L. Lastras-Martínez, R. Balderas-Navarro, R. López-Estropier, A. Lastras-Martínez, *Appl. Surf. Sci.* **2018**, *439*, 963.
- [68] H. Hughes, C. Springer, U. Resch, N. Esser, W. Richter, *J. Appl. Phys.* **1995**, *78*, 1948.
- [69] G. Sombrio, E. Oliveira, J. Strassner, C. Doering, H. Fouckhardt, *J. Vac. Sci. Technol.* **2021**, *39*, 052204.
- [70] S. Brückner, P. Kleinschmidt, O. Supplie, H. Döschner, T. Hannappel, *New J. Phys.* **2013**, *15*, 113049.
- [71] N. Witkowski, R. Coustel, O. Pluchery, Y. Borensztein, *Surf. Sci.* **2006**, *600*, 5142.
- [72] M. M. May, O. Supplie, C. Höhn, R. van de Krol, H.-J. Lewerenz, T. Hannappel, *New J. Phys.* **2013**, *15*, 103003.
- [73] A. Baghbanpourasl, W. G. Schmidt, M. Denk, C. Cobet, M. Hohage, P. Zeppenfeld, K. Hingerl, *Surf. Sci.* **2015**, *641*, 231.
- [74] M. M. May, H. Stange, J. Weinrich, T. Hannappel, O. Supplie, *SciPost Phys.* **2019**, *6*, 58.
- [75] M. M. May, H.-J. Lewerenz, D. Lackner, F. Dimroth, T. Hannappel, *Nat. Commun.* **2015**, *6*, 8286.
- [76] B. L. Pearce, S. J. Wilkins, T. Paskova, A. Ivanisevic, *J. Mater. Res.* **2015**, *30*, 2859.
- [77] C. I. Smith, N. J. Almond, P. Weightman, *J. Electrochem. Soc.* **2007**, *154*, F90.
- [78] H. Gerischer, *Electrochim. Acta* **1990**, *35*, 1677.
- [79] C. I. Smith, P. Harrison, T. Farrell, P. Weightman, *J. Phys. Condens. Matter* **2012**, *24*, 482002.
- [80] P. Harrison, C. I. Smith, Y. Gründer, C. A. Lucas, S. D. Barrett, P. Weightman, *Phys. Chem. Chem. Phys.* **2016**, *18*, 24396.

- [81] B. Sheridan, D. S. Martin, J. R. Power, S. D. Barrett, C. I. Smith, C. A. Lucas, R. J. Nichols, P. Weightman, *Phys. Rev. Lett.* **2000**, *85*, 4.
- [82] O. Magnussen, J. Wiechers, R. Behm, *Surf. Sci.* **1993**, *289*, 139.
- [83] R. Michaelis, D. Kolb, *Surf. Sci.* **1990**, *234*, L281.
- [84] V. Mazine, Y. Borensztein, *Phys. Rev. Lett.* **2002**, *88*, 147403.
- [85] V. Mazine, *Phys. Status Solidi* **1999**, *6*.
- [86] T. Yamada, K. Shirasaka, A. Takano, M. Kawai, *Surf. Sci.* **2004**, *561*, 233.
- [87] P. D. Lane, G. E. Isted, R. J. Cole, *Phys. Status Solidi B* **2010**, *247*, 1969.
- [88] X. F. Jin, M. Y. Mao, S. Ko, Y. R. Shen, *Phys. Rev. B* **1996**, *54*, 7701.
- [89] L. Sun, M. Hohage, P. Zeppenfeld, R. Balderas-Navarro, K. Hingerl, *Phys. Rev. Lett.* **2003**, *90*, 106104.
- [90] C. Punckt, F. S. Merkt, H. H. Rotermund, *New J. Phys.* **2007**, *9*, 213.
- [91] G. Barati, V. Solokha, K. Wandelt, K. Hingerl, C. Cobet, *Langmuir* **2014**, *30*, 14486.
- [92] C. Goletti, G. Bussetti, A. Violante, B. Bonanni, M. Di Giovannantonio, G. Serrano, S. Breuer, K. Gentz, K. Wandelt, *J. Phys. Chem. C* **2019**, *119*, 1782.
- [93] S. Vazquez-Miranda, V. Solokha, R. E. Balderas-Navarro, K. Hingerl, C. Cobet, *J. Phys. Chem. C* **2020**, *124*, 5204.
- [94] G. Jerkiewicz, *Electrocatal* **2010**, *1*, 179.
- [95] R. Yivlialin, C. Filoni, F. Goto, A. Calloni, L. Duò, F. Ciccacci, G. Bussetti, *Molecules* **2022**, *27*, 8010.
- [96] Z. Chen, P. Gao, W. Wang, S. Klyatskaya, Z. Zhao-Karger, D. Wang, C. Kübel, O. Fuhr, M. Fichtner, M. Ruben, *ChemSusChem* **2019**, *12*, 3737.
- [97] M. M. May, W. Jaegermann, *Curr. Opin. Electrochem.* **2022**, *34*, 100968.
- [98] P. P. Notten, *Electrochemical study of the etching of III-V semiconductors*, Technische Universiteit Eindhoven **1989**.
- [99] H.-J. Lewerenz, I. D. Sharp, *Chapter 1. Concepts of Photoelectrochemical Energy Conversion and Fuel Generation*, Royal Society of Chemistry **2018**.
- [100] S. E. Acosta-Ortiz, A. Lastras-Martínez, *Phys. Rev. B* **1989**, *40*, 1426.
- [101] T. Bruhn, B.-O. Fimland, M. Kneissl, N. Esser, P. Vogt, *Phys. Rev. B* **2011**, *83*, 045307.
- [102] A. Goryachev, L. Gao, R. P. J. van Veldhoven, J. E. M. Haverkort, J. P. Hofmann, E. J. M. Hensen, *Phys. Chem. Chem. Phys.* **2018**, *20*, 14242.
- [103] K. Schulte, H. Lewerenz, *Electrochim. Acta* **2002**, *47*, 2633.
- [104] H. Lewerenz, K. Schulte, *Electrochim. Acta* **2002**, *47*, 2639.
- [105] C. I. Smith, P. Harrison, C. A. Lucas, Y. Grunder, S. D. Barrett, P. Weightman, *J. Phys. Condens. Matter* **2016**, *28*, 015005.
- [106] B. M. Ocko, A. Gibaud, J. Wang, *J. Vac. Sci. Technol.* **1992**, *10*, 3019.
- [107] D. M. Kolb, J. Schneider, *Electrochim. Acta* **1986**, *31*, 929.
- [108] D. Kolb, *Prog. Surf. Sci.* **1996**, *51*, 109.
- [109] I. R. de Moraes, F. C. Nart, *J. Electroanal. Chem.* **1999**, *461*, 110.
- [110] O. M. Magnussen, J. Hageböck, J. Hotlos, R. J. Behm, *Faraday Discuss.* **1992**, *94*, 10.
- [111] Z. Shi, J. Lipkowski, *J. Electroanal. Chem.* **1996**, *403*, 225.
- [112] C. I. Smith, A. Bowfield, N. J. Almond, C. P. Mansley, J. H. Convery, P. Weightman, *J. Phys. Condens. Matter* **2010**, *22*, 392001.
- [113] A. El Kharbachi, O. Zavorotynska, M. Latroche, F. Cuevas, V. Yartys, M. Fichtner, *J. Alloys Compd.* **2020**, *817*, 153261.
- [114] Q. Zhao, S. Stalin, L. A. Archer, *Joule* **2021**, *5*, 1119.
- [115] A. M. Tripathi, W.-N. Su, B. J. Hwang, *Chem. Soc. Rev.* **2018**, *47*, 736.
- [116] Y. Liang, H. Dong, D. Aurbach, Y. Yao, *Nat. Energy* **2020**, *5*, 646.
- [117] F. Maroni, S. Dongmo, C. Gauckler, M. Marinaro, M. Wohlfahrt-Mehrens, *Batteries & Supercaps* **2021**, *4*, 1221.
- [118] J. Shi, J. Zhang, J. Guo, J. Lu, *Nanoscale Horiz.* **2020**, *5*, 1467.
- [119] Z. Lu, A. Schechter, M. Moshkovich, D. Aurbach, *J. Electroanal. Chem.* **1999**, *466*, 203.
- [120] B. E. Hayden, E. Schweizer, R. Kötz, A. M. Bradshaw, *Surf. Sci.* **1981**, *111*, 26.
- [121] Z. Zhao-Karger, M. E. G. Bardaji, O. Fuhr, M. Fichtner, *J. Mater. Chem. A* **2017**, *5*, 10815.
- [122] L. A. Kibler, *Int. S. of Electrochem.* **2003**.
- [123] M. Schlipf, F. Gygi, *Comput. Phys. Commun.* **2015**, *196*, 36.
- [124] M. Löw, M. Guidat, J. Kim, M. M. May, Zenodo dataset for "The interfacial structure of InP(100) in contact with HCl and H₂SO₄ studied by reflection anisotropy spectroscopy" **2022**, DOI: 10.5281/zenodo.7410144.
- [125] J. Kim, NOMAD dataset: RAS InP100 with Cl and H **2023**, DOI: 10.17172/NOMAD/2023.01.16-1.

Manuscript received: January 20, 2023

Revised manuscript received: February 23, 2023

Version of record online: March 22, 2023